International Journal of Heat and Fluid Flow 29 (2008) 1670–1678

Contents lists available at ScienceDirect

International Journal of Heat and Fluid Flow

journal homepage: www.elsevier.com/locate/ijhff

Study of the blowing impact on a hot turbulent boundary layer using Thermal Large Eddy Simulation

G. Brillant [a,b], S. Husson [b], F. Bataille [b,*], F. Ducros [a]

[a] CEA/Grenoble DEN/DER/SSTH/LMDL, 17 rue des Martyrs 38054, Grenoble Cedex 9, France
[b] INSA/Centre de Thermique de Lyon (UMR CNRS 5008), Bat. Sadi Carnot 69621, Villeurbanne Cedex, France

ARTICLE INFO

Article history:
Received 16 July 2007
Received in revised form 1 June 2008
Accepted 27 June 2008
Available online 3 September 2008

Keywords:
Thermal Large Eddy Simulation
Turbulent inflow conditions
Blowing
Wall heat transfer

ABSTRACT

We investigate Thermal Large Eddy Simulation in a complex case using Trio U. We develop a thermal turbulent inflow condition based on parallel flows in order to simulate a turbulent thermal boundary layer. This inflow condition is tested with a turbulent channel flow. We show that it produces fine profiles for velocity and temperature. Later, this inlet condition is used in the case of blowing through a porous plate. Two different blowing regimes are studied: the classical turbulent boundary layer and the blown off boundary layer. Comparisons show that we obtain similar experimental and numerical profiles (Brillant, G., Husson, S., Bataille, F., 2008. Experimental study of the blowing impact on a hot turbulent boundary layer. International Journal of Heat and Mass Transfer 51 (7–8), 1996–2005.). We finish with additional results obtained only through numerical simulations.

1. Introduction

In the last decades, Large Eddy Simulation (LES) has been more and more widely developed. In his general presentation of turbulence, Lesieur (1997) considers LES as a necessary and very promising tool to study turbulent flows. The formalism of LES in the incompressible case is presented by Sagaut (2001), who also gives a comprehensive review of the modelling techniques for the subgrid stress tensor as well as an overview of the important points related to LES (numerical methods, boundary conditions, etc.). Near-wall modelling in LES has been investigated in particular by Piomelli and Balaras (2002). LES can now be used for intricate studies (Erlebacher et al., 1992; Moin, 2002; Mellen et al., 2003; Rodi, 2006). Recently, some LES studies involving heat transfer have been conducted. Dong and Lu (2004) applied LES to a thermally stratified turbulent channel and studied the effects of temperature oscillations on the lower wall. Wang and Pletcher (1996) investigated the influence of fluid properties variations in a turbulent channel flow with significant heat transfer. Murata and Mochizuki (2004a,b) studied turbulent heat transfer in a two-pass square channel. Lee et al. (2004) carried out simulations in a vertical channel with several temperature differences to study the coupling of fluid properties variations and gravity. Chatelain et al. (2004) investigated numerical schemes for LES of heat transfer. Several authors developed and assessed subgrid-scale models for the subgrid heat flux. Moin et al. (1991) extended the dynamic procedure proposed by Germano et al. (1991) to the subgrid heat flux modelling. Tensorial models have been developed for the subgrid diffusivity (Montreuil et al., 1999; Peng and Davidson, 2002). Sergent et al. (2003) developed a mixed scale model for the simulation of natural convection flows. Nevertheless, there are less studies related to thermal LES than dynamic LES, and many questions related to thermal LES are still pending. Some studies are missing, especially in industrial configurations, where non-isothermal turbulent wall flows are often encountered (combustion chambers, T-junctions, turbines). We describe hereafter a thermal turbulent inlet that make such a simulation possible. We simulate the flow over a porous plate submitted to blowing to assess this inflow condition.

The simulation of a turbulent flow is strongly dependent on the conditions at the inlet. Special care is required in defining such conditions in order to produce some turbulent boundary layers and to carry out some large eddy simulations. Several methods have been developed for the velocity. One method adds fluctuations to a laminar profile. It involves simulation of the laminar–turbulent transition, which is difficult and expensive (Ducros et al., 1996; Rai and Moin, 1993). Another method adds random fluctuations to a mean turbulent profile (Le et al., 1997; Lee et al., 1992). However, the simulated profiles can differ from the physical ones as fluctuations are random. Such problem can be avoided with an inlet condition based on parallel flows leading to profiles that are sound (Akselvoll and Moin, 1996; Brillant et al., 2004; Kaltenbach et al., 1999). A recycling method can also be used. It is based on a

* Corresponding author. Current address: PROMES/CNRS, Rambla de la thermodynamique, Tecnosud, 66100 Perpignan, France. Tel.: +33 4 68 68 22 32; fax: +33 4 68 68 22 13.
E-mail address: Francoise.Daumas-Bataille@univ-perp.fr (F. Bataille).

0142-727X/$ - see front matter © 2008 Elsevier Inc. All rights reserved.
doi:10.1016/j.ijheatfluidflow.2008.06.011

Nomenclature

F	blowing rate (injection rate), %
g	gravity, m s^{-2}
h	channel half height, m
P	pressure, Pa
Q	Q criterion, s^{-2}
Re	Reynolds number based on the main velocity and the length of the plate
Re_τ	Reynolds number based on the friction velocity and the channel half height
S_{ij}	strain tensor, s^{-1}
T	temperature, K
t	time, s
U_τ	friction velocity $U_\tau = \sqrt{\tau_w/\rho}$, m s^{-1}
U	velocity, m s^{-1}
u, v, w	velocity components in x, y, z directions, m s^{-1}
x, y, z	Cartesian coordinates, m

Greek symbols

β	compressibility coefficient, K^{-1}
δ_{ij}	Kronecker symbol
κ	thermal diffusivity, m^2 s^{-1}
ν	kinematic viscosity, m^2 s^{-1}
Ω_{ij}	rotation tensor, s^{-1}
π_{jT}	subgrid-scale heat flux, K m s^{-1}
ρ	density, kg m^{-3}
τ_w	wall shear stress: $\tau_w = \rho\nu\partial\overline{U}/\partial y\|_{y=0}$, kg m^{-1} s^{-2}
τ_{ij}	subgrid-scale stress tensor, m^2 s^{-2}

Subscripts and superscripts

∞	variable related to the flow far from the wall (main hot-flow)
inj	variable related to the injected fluid (cold fluid)
ref	reference value
sgs	subgrid-scale variable
m	mean value
rms	root mean square value
$-$	filtered variable
+	non-dimensional variable

variable transformation to limit the calculation cost (Lund and Moin, 1996; Wu et al., 1995).

The aim of the present work is to investigate Thermal Large Eddy Simulation in some intricate case. Past studies limited to the velocity field their investigations on the definition of a turbulent inflow condition. Similar work is required with the temperature field in thermal LES. Continuing some published work (Brillant et al., 2004), we developed a thermal turbulent inflow condition based on parallel flows for the simulation of a turbulent thermal boundary layer. We first tested this inflow condition with a turbulent channel flow. Then we considered the case of blowing through a porous plate.

Blowing consists of cold fluid injection through a porous material. It is a very efficient technique to protect surfaces exposed to high temperatures (Bellettre et al., 2000; Facchini et al., 2000). Both experimental (Bellettre et al., 1999) and numerical (Merkin, 1972, 1975; Mathelin et al., 2001a,b; Shima, 1993; Silva-Freire et al., 1995) studies on blowing have been reported. Study of heat transfer with LES would provide us some insights on the impact of blowing on the temperature fluctuations or on the temperature–velocity correlations. Previous work provides us with the necessary experimental data to validate our results (Brillant et al., 2008). Conversely, we assess the developments of thermal LES with cases that involve blowing.

In the present study, we consider a turbulent boundary layer disturbed by the injection of a cold fluid through a plane porous plate (see Fig. 1a). Experimental measurements (Brillant et al., 2008) are used as a comparison to validate the method. In the experimental configuration, the turbulent boundary layer develops along an impermeable wall that precedes the porous plate. We consider only the flow above the porous plate in order to reduce the calculation time and to avoid the simulation of the transition to turbulence. It is indeed very difficult to reproduce correctly this transition. We can solve this problem with the use of a turbulent inlet. Only the last two centimeters of impermeable wall are included in the calculation domain as a development length for our turbulent inlet. The Reynolds number based on the mean flow velocity is $Re \approx 750{,}000$ at the beginning of the porous plate. The porous plate is 35 cm long, with a porosity of 33%. The cold and hot fluid are gas (air). The main hot flow velocity is fixed to $U_\infty = 10$ m s^{-1} and the cold flow injection is characterized by the blowing rate:

$$F = \frac{\rho_{inj} U_{inj}}{\rho_\infty U_\infty}. \quad (1)$$

Four blowing rates ($F = 0.5\%$, $F = 1\%$, $F = 2\%$ and $F = 5\%$) have been simulated. The temperature of the cold flow is the ambient temperature (293 K). In the future we will use LES with high temperature differences but in this study we first focus on a case where the Boussinesq hypothesis is valid. Consequently, we set the temperature of the main flow to 313 K. The temperature gap between the main and injected flows is equal to $\Delta T = 20$ K.

First, we describe the schemes, models and methods used in the simulations. Then, we focus on the definition of our thermal turbulent inlet and the presentation of some test cases. Finally, we compare and discuss in details our numerical results with experimental measurements on the blowing configuration.

2. Numerical setup

Large eddy simulations are carried out using the Trio U code. It is mostly developed by the French atomic energy agency (CEA). Two and three dimensional thermohydraulic calculations can be conducted with several kinds of discretization and different kinds of fluid. The code can deal with both laminar and turbulent flows. We use the finite difference volume discretization. The filtered Navier–Stokes equations are solved for an incompressible flow with the Boussinesq hypothesis:

$$\frac{\partial \bar{u}_j}{\partial x_j} = 0, \quad (2)$$

$$\frac{\partial \bar{u}_i}{\partial t} + \frac{\partial \bar{u}_i \bar{u}_j}{\partial x_j} = -\frac{1}{\rho}\frac{\partial \overline{P}}{\partial x_i} + \nu\frac{\partial^2 \bar{u}_i}{\partial^2 x_j} - \frac{\partial \tau_{ij}}{\partial x_j} + \beta(\overline{T} - T_{ref})g_i, \quad (3)$$

$$\frac{\partial \overline{T}}{\partial t} + \frac{\partial \overline{T}\bar{u}_j}{\partial x_j} = \kappa\frac{\partial^2 \overline{T}}{\partial^2 x_j} - \frac{\partial \pi_{jT}}{\partial x_j}, \quad (4)$$

where j is the summation subscript and i represents the velocity component. $\tau_{ij} = \overline{u_i u_j} - \bar{u}_i \bar{u}_j$ is the subgrid-scale stress tensor and $\pi_{jT} = \overline{T u_j} - \overline{T}\bar{u}_j$ is the subgrid-scale heat flux. Both are modeled using the concept of eddy viscosity ν_{sgs} and eddy diffusivity κ_{sgs}:

$$\tau_{ij} - \frac{1}{3}\delta_{ij}\tau_{kk} = -2\nu_{sgs}\bar{S}_{ij}, \quad (5)$$

$$\pi_{jT} = -\kappa_{sgs}\frac{\partial T}{\partial x_j}, \quad (6)$$

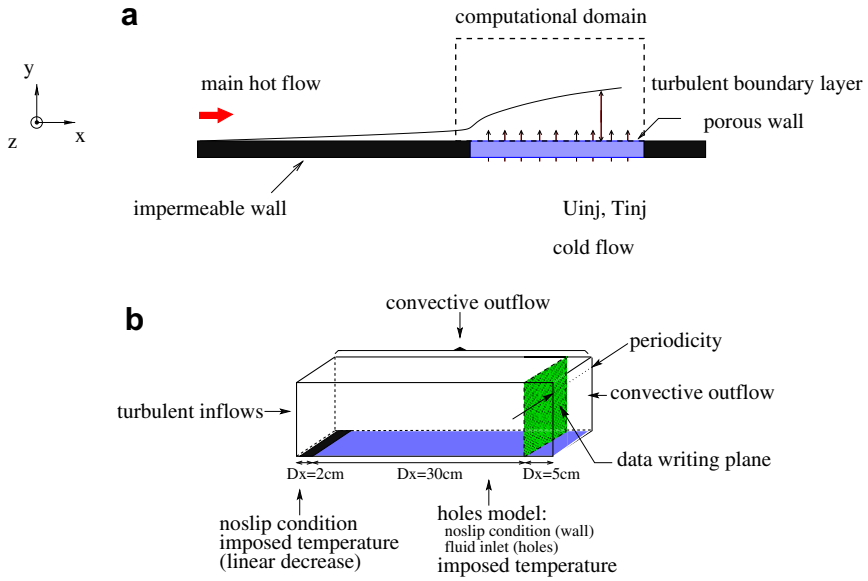

Fig. 1. Studied configuration (a) and boundary conditions (b).

where

$$\bar{S}_{ij} = \frac{1}{2}\left(\frac{\partial \bar{u}_i}{\partial x_j} + \frac{\partial \bar{u}_j}{\partial x_i}\right). \tag{7}$$

The eddy viscosity is expressed by the WALE model developed by Nicoud and Ducros (1999). This model is based on both the strain and rotation tensors and has the appropriate wall behaviour ($\nu_{sgs} \propto y^3$). We use a model that correctly reproduces the no-slip condition at the wall since no wall-law is used and a fine mesh is built near the plate. For the eddy diffusivity, the hypothesis of a constant subgrid-scale Prandtl number ($Pr_{sgs} = \nu_{sgs}/\kappa_{sgs} = 0.9$) is considered. It is a first step for the LES of non-isothermal blowing even though this model is quite simple. Furthermore, previous simulations in a turbulent plane channel with this model gave good results and did not show significant differences with a dynamic thermal diffusivity model.

Time integration is carried out by a third order Runge–Kutta scheme. The convection scheme for the momentum equation is a second order centered scheme. Previous tests showed that the results obtained with the second order scheme are accurate (Ackermann and Métais, 2001; Brillant et al., 2004) although a higher order scheme could be considered. When centered schemes are considered for energy equation, temperature fluctuations are quite well estimated but instantaneous temperature is observed to reach values that are out of the physical range (Chatelain et al., 2004). Therefore, a third order quick scheme has been employed in the following even if numerical diffusion will lead to under-estimated temperature fluctuations.

The dimensions of the computational domain are: $L_x = 0.37$ m, $L_y = 0.12$ m, $L_z = 0.03$ m. In the plane $y = 0.00$ m, we consider an impermeable wall from $x = 0.00$ m to $x = 0.02$ m and a porous plate from $x = 0.02$ m to $x = 0.37$ m. The simulation results at the plane $x = 0.32$ m (30 cm after the beginning of the porous plate) are extracted and compared to the experimental ones. The transverse dimension is chosen in order to avoid correlation between the data of each boundary (Moin and Kim, 1982; Jiménez and Moin, 1991). The mesh consists in $186 \times 50 \times 31$ nodes. We constructed a gradual mesh along the vertical axis in order to apply a no-slip condition at the wall while limiting the calculation time. It is refined at the wall ($y^+ \simeq 1$) and it widens following a hyperbolic tangent progression:

$$y_k = L_y\left\{1 + \frac{1}{a}\tanh\left[\left(-1 + \frac{(k-1)}{N_y - 1}\right)\operatorname{atanh}(a)\right]\right\}, \quad k \in [1, N_y], \tag{8}$$

where N_y is the number of nodes along the vertical axis and a is a constant number, which defines the dilation of the mesh. The mesh is uniform along the longitudinal and transverse axis. The non-dimensional mesh spacings, $\Delta x^+ \approx 50$ and $\Delta z^+ \approx 40$, correspond to a moderate resolution.

We use a "holes model" developed by Bellettre et al. (1999) to represent the porous plate (from $x = 0.02$ m to $x = 0.37$ m). It consists in a succession of walls and holes. The number of wall elements is twice the number of holes to fit the porosity of the experimental plate (30%). The size of each element is 2 mm. That corresponds to the longitudinal mesh spacing. It is much bigger than the size of the pores of the real material (30 μm). Nevertheless, previous work showed that good results can be obtained with this value (Bellettre et al., 1999, 2000).

All the boundary conditions employed in our study are displayed in Fig. 1b. A no-slip condition is applied to the velocity along the first two centimeters of impermeable wall and along the wall elements of the holes model. The holes are associated to the cold fluid inlet, with a velocity depending on the blowing rate. The temperature of the porous plate is set to the experimental one for both walls and holes elements ($T_{F=0.5\%} = 305.8$ K, $T_{F=1\%} = 299.6$ K, $T_{F=2\%} = 295.0$ K and $T_{F=5\%} = 293.2$ K). Periodic conditions are imposed to the transverse boundaries. The upper and exit boundary conditions are convective outflows. For the upper limit, a symmetry condition could not be considered as the mean and fluctuating parts of the vertical velocity are not negligible.

We consider a turbulent inflow condition based on parallel flows in order to obtain a developed turbulent dynamic boundary layer at the beginning of the porous plate. It has been developed and previously tested (Brillant et al., 2004). This inflow, applied to the three components of the velocity, produces appropriate mean and turbulent velocity profiles that do not deteriorate along the domain (Brillant et al., 2004). We have adapted this turbulent inflow condition to the temperature for the thermal inlet. The temperature at the beginning of the impermeable wall is $T_{x=0,y=0} = 311.9$ K. It depends on the thermal inlet and it is set by the experimental mean profile. We interpolate the temperature along

the impermeable wall from $x = 0$ to $x = 0.02$ m in order to avoid any temperature jump at the beginning of the porous plate. We give in the next section the characteristics and test cases of this thermal inflow condition.

3. Thermal inlet condition

We use an additional domain to generate a thermal turbulent profile. This domain provides the fluctuations that we apply to the inlet of the main domain (porous plate submitted to blowing). The additional domain is a turbulent plane channel. While the mean temperature profile at inlet was taken directly from experiment (2 cm before the porous plate), the instantaneous fluctuating temperature profile was obtained by running an LES of fully developed thermal channel flow for the same Reynolds number (using just one half of the profile). The entering instantaneous temperature for the main calculation was thus obtained adding, at all points on the entry plane, the local measured mean temperature to the fluctuating temperature obtained from the channel LES.

We consider the same fluid to obtain similar profiles in both domains (plane channel and porous plate with blowing). We use previous experimental data (Brillant et al., 2008) to define the channel. The friction velocity of the channel is set to the experimental friction velocity of the porous plate ($U_\tau \simeq 0.39$ m s^{-1}). The Reynolds number based on the friction velocity is $Re_\tau \simeq 380$. The channel dimensions are $2\pi h \times 2h \times \pi h$, with $h \simeq 0.0149$ m; its non-dimensional lengths are $L_x^+ \simeq 2500$, $L_y^+ \simeq 760$ and $L_z^+ \simeq 1250$. A mesh with $64 \times 65 \times 32$ nodes is constructed. The mesh for the porous plate is uniform along the longitudinal and transverse axis but it is refined near the walls along the vertical axis, following a hyperbolic tangent transformation. The non-dimensional mesh spacings are $\Delta_x^+ \simeq 40$, $\Delta_y^+ \simeq 1$ at the wall, $\Delta_y^+ \simeq 15$ at the centerline and $\Delta_z^+ \simeq 40$. The channel is periodic in the longitudinal and transverse directions. A no-slip condition is applied to the velocity at the walls. The top wall of the channel is adiabatic and we impose at the bottom wall the same heat flux as in the blowing configuration. It is given by the experimental data ($\Phi = -13.4$ W m^{-2}). A source term ($S = 447$ W m^{-3}) is added in the whole domain for energy conservation purpose.

Initially, a simulation was carried out with the turbulent inlet for the three components of the velocity but only a mean profile (no fluctuations) as temperature inlet to prove the need of such a turbulent thermal inlet. A turbulent plane channel was considered as main domain instead of the porous plate. In Fig. 2, we can see that the turbulent velocity field does not generate thermal fluctuations quickly. The temperature fluctuations profile is not yet established at $x = 5h$. We note that at the lower wall, where a constant heat flux is imposed, the fluctuations level increases slowly. At the top wall, which is adiabatic, the level remains low. An analysis of the energy equation explains these observations. The effect of the velocity in the energy equation (Eq. (4)) appears in the convection term: $\bar{u}_j \frac{\partial \bar{T}}{\partial x_j}$. With the imposed heat flux $\frac{\partial \bar{T}}{\partial x} = \frac{\partial \bar{T}}{\partial z} = 0$ but $\frac{\partial \bar{T}}{\partial y} \neq 0$. Therefore, the velocity has an influence on the temperature, but only through its vertical component v. That is why there is a slow evolution of the temperature fluctuations due to the turbulent velocity. With the adiabatic wall $\frac{\partial \bar{T}}{\partial x} = \frac{\partial \bar{T}}{\partial y} = \frac{\partial \bar{T}}{\partial z} = 0$. The velocity can hardly influence the temperature in this case. Consequently the thermal fluctuation do not develop by means of the velocity fluctuations. This analysis also shows that we have to apply the turbulent dynamic inlet to the three components of the velocity in order to maintain the temperature fluctuations level. It is not sufficient to consider only the longitudinal one.

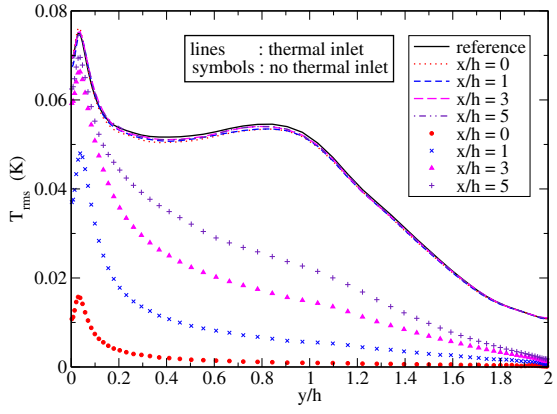

Fig. 2. Temperature fluctuations in the main turbulent plane channel with and without the turbulent thermal inlet (the reference profiles are the fully developed profiles in the plane channel).

The thermal inlet generation method was then tested with a plane channel as main domain. We intended to check that it generates temperature fluctuations at the entry of the main domain and it maintains them along this domain. This inlet is very efficient as shown in Fig. 2. The fluctuating temperature profiles are identical to the expected ones (fully developed channel flow) at the entry of the second channel and they remain constant downstream.

We also carried out a test with the blowing configuration as main domain to see whether the fluctuations extracted from the channel would give the appropriate profiles when the main domain consists of a spatially evolving boundary layer. The comparison of the numerical profiles with the experimental ones just before the porous plate in Fig. 3 shows that our turbulent thermal and dynamic inlets produce the expected profiles on the flat plate. Moreover, we note that they require only a short transition zone, since the profiles are established after only 1 cm. We used this method for the simulations of the porous plate submitted to blowing in order to obtain appropriate turbulent inflow conditions. The results are discussed in the next section.

4. Results

We compare our numerical results to the experimental measurements presented in a previous article (Brillant et al., 2008). We focus here on the agreement of the numerical profiles with the experimental ones since the impact of blowing has already been well discussed in that paper. We separated the results obtained with a blowing rate $F = 5\%$ from the others since they are peculiar. We first validate the simulations for blowing rates $F \leqslant 2\%$. We also present some new results given exclusively by the simulations. The case $F = 5\%$ is discussed afterwards.

4.1. Simulations for $F \leqslant 2\%$: classic turbulent boundary layer

The comparison of the mean profiles for the longitudinal velocity and the temperature in Figs. 4a and 5a shows a quite good agreement between the simulations and the experiments. We notice in Fig. 4a that the simulations under-estimate the mean vertical velocity. However, the trends of the numerical profiles are similar to the experimental ones and the maxima appear at the same distance from the wall in both cases. Moreover, the vertical velocity is found to increase with the blowing rate, as in the experiments. The discrepancies in the vertical velocity level may originate from both experimental and numerical errors. Experimentally, the determination of the vertical velocity using a crossed hot wires probe is very sensitive to the value of the angle between the wires and the vertical direction. Small inaccuracies in the measure of this angle lead to significant changes in the experimental values of the vertical velocity. In a numerical point of view, the vertical component of the velocity is the most sensitive to this fluid

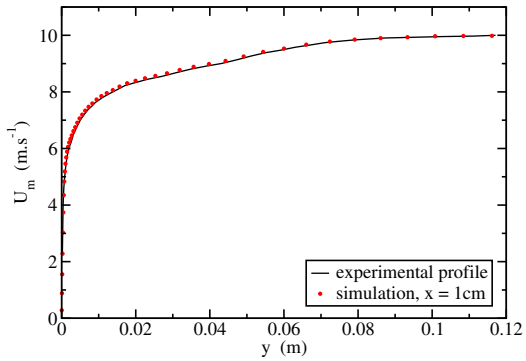

(a) Mean longitudinal velocity.

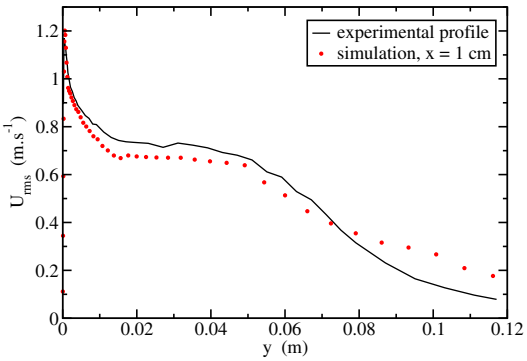

(b) Root mean square of the longitudinal velocity.

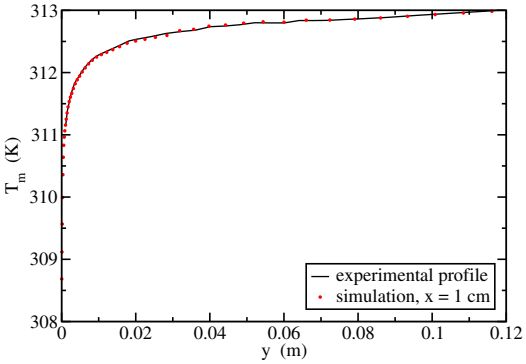

(c) Mean temperature.

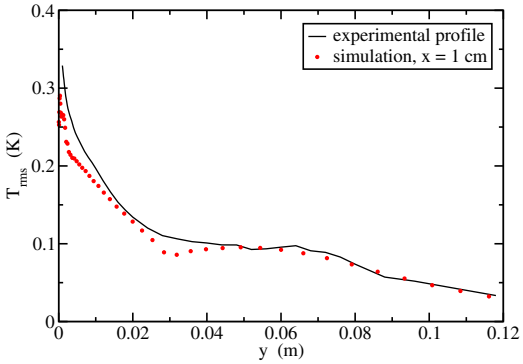

(d) Root mean square of the temperature.

Fig. 3. Velocity and temperature profiles 1 cm before the porous plate.

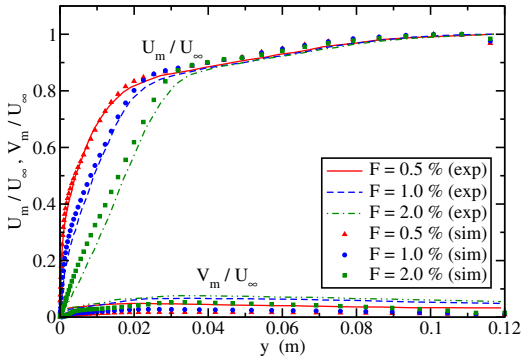

(a) Mean longitudinal and vertical velocity.

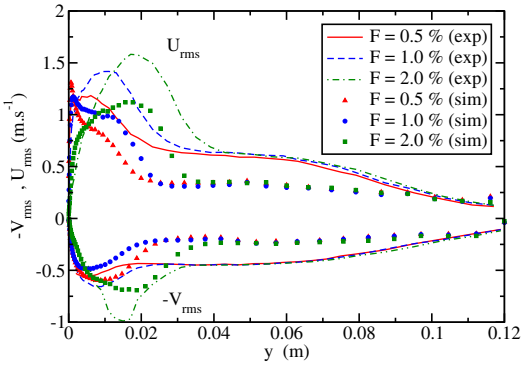

(b) Root mean square of the longitudinal and vertical velocity.

Fig. 4. Longitudinal and vertical velocity profiles ($F \leqslant 2\%$).

inlet condition, since the cold fluid is injected vertically. Thus, the impact of the holes model used to represent the porous plate is greater on the vertical velocity than on the longitudinal one. The hot turbulent inlet used in our simulations may also have an influence on the vertical velocity. This inlet is extracted from a channel where the boundary layer is established, whereas in the main domain the boundary layer evolves spatially along the wall. This difference may affect the vertical velocity profiles.

The velocity and temperature fluctuations are displayed in Figs. 4b and 5b. The shapes of the numerical profiles are identical to the experimental ones. In particular, the positions of the maxima correspond quite well. The evolution of the profiles with the blowing rate is also similar in both cases: the maxima of the fluctuations increase and the peaks widen. Even if the order of magnitude of velocity and temperature fluctuations is correctly estimated by calculations, we note an overall under-estimation that is more pronounced for vertical velocity (about a factor 2). Discrepancies may mainly come from the hole model, the numerical diffusion of quick scheme used for energy equation and the turbulent inlet condition (that cannot reproduce all characteristic of an evolving turbulent boundary layer, especially concerning fluctuations). Besides, velocity fluctuations have been observed in turbulent channel flow to be highly sensitive to grid resolution and notably resolution along z axis. Therefore, improvements may be allowed with bigger simulations. We observe undesirable peaks close to the wall for $F = 0.5\%$ and $F = 1\%$ on the longitudinal velocity

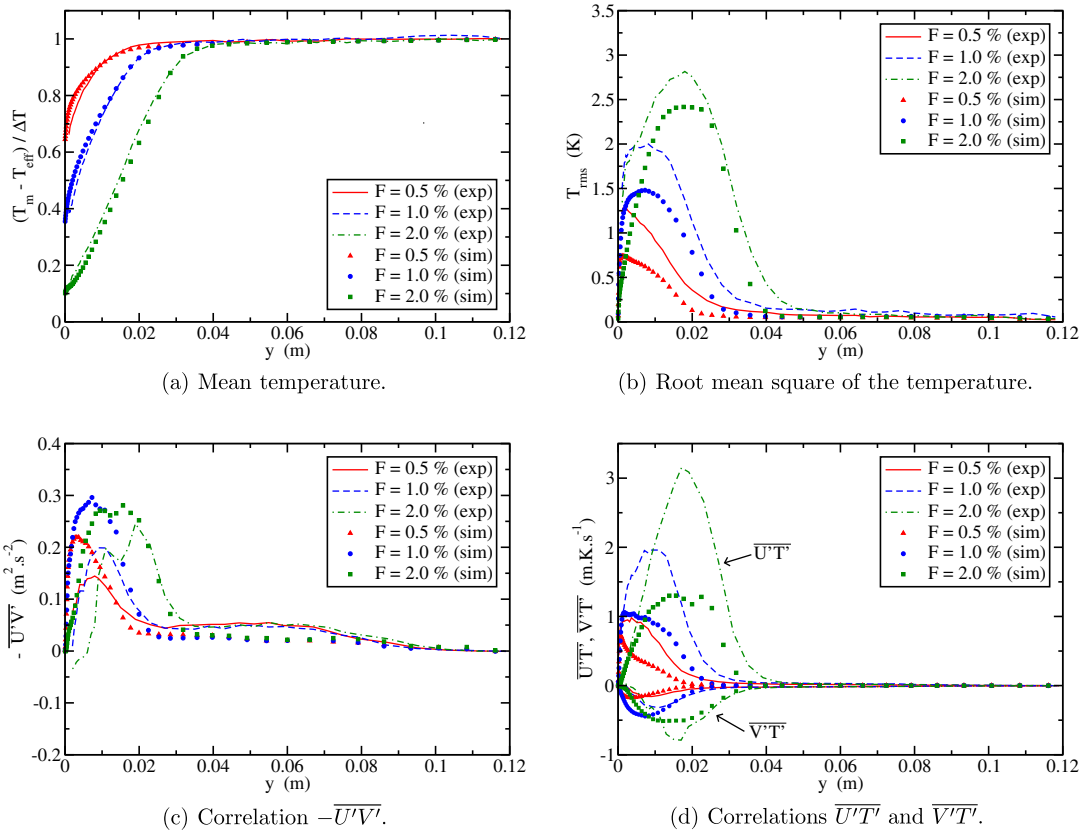

(a) Mean temperature. (b) Root mean square of the temperature.

(c) Correlation $-\overline{U'V'}$. (d) Correlations $\overline{U'T'}$ and $\overline{V'T'}$.

Fig. 5. Temperature and correlations profiles ($F \leqslant 2\%$).

fluctuation profiles. They are attributed to the difficulty of reproducing numerically the blowing process when the injection rate is too low to clearly move the flow away from the wall. This problem disappears with other velocity fluctuations.

The velocity–velocity and velocity–temperature correlations are displayed in Fig. 5c and d. Even if order of magnitude and shape are roughly well reproduced by simulations, the calculated profiles are observed to not fit experimental ones. Differences may be partially explained by the blowing model used in our study which is quite simple. In fact, injection rate F is correctly imposed in our calculations but not the ratio of the injected momentum to streamwise momentum. A more elaborated blowing model will consequently be useful in a future study. One way could be the use of velocity momentum and heat flux sources (which takes into account blowing injection in more than one direction) in cell bounding a wall no-slip condition.

Numerical approach of blowing impact on a turbulent boundary layer confirms experimental observations discussed in Brillant et al. (2008). Concerning mean values of velocity and temperature, the good agreement between experimental and numerical results validates our simulations for $F \leqslant 2\%$. Nevertheless, even if the shape of velocity and temperature fluctuations profiles are quite well reproduced by calculations, enhancements can be expected, in a further work, concerning a quantitative fluctuations level estimation.

4.2. Additional results given by the simulations for $F \leqslant 2\%$

The simulations conducted in the present study permit us to obtain new results that were not given by the experimental measurements. As shown in Fig. 6, we can plot the transverse velocity fluctuations. We notice that the maximum of these fluctuations increases and is pushed away from the wall when the blowing rate

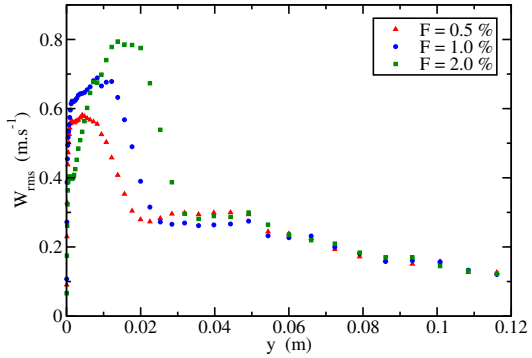

Fig. 6. Root mean square of the transverse velocity ($F \leqslant 2\%$).

increases. This behaviour is similar to the behaviour of the other velocity fluctuations presented previously.

We can estimate the impact of blowing on the turbulent structures of the flow by means of the Q criterion (Dubief and Delcayre, 2000). This criterion is defined by

$$Q = \frac{1}{2}\left(\overline{\Omega}_{ij}\overline{\Omega}_{ij} - \overline{S}_{ij}\overline{S}_{ij}\right) \tag{9}$$

where S_{ij} and Ω_{ij} are, respectively, the strain and the rotation tensor.

Isosurfaces of the Q criterion with a threshold of 50,000 s^{-2} are represented for different blowing rates in Fig. 7. We notice that the amount of vortices increases with the blowing rate. Moreover, the area where these structures develop becomes larger. These remarks confirm the tendency observed with the velocity fluctuations profiles: blowing increases the level of the fluctuations and enlarges their peak, shifting their maximum away from the wall.

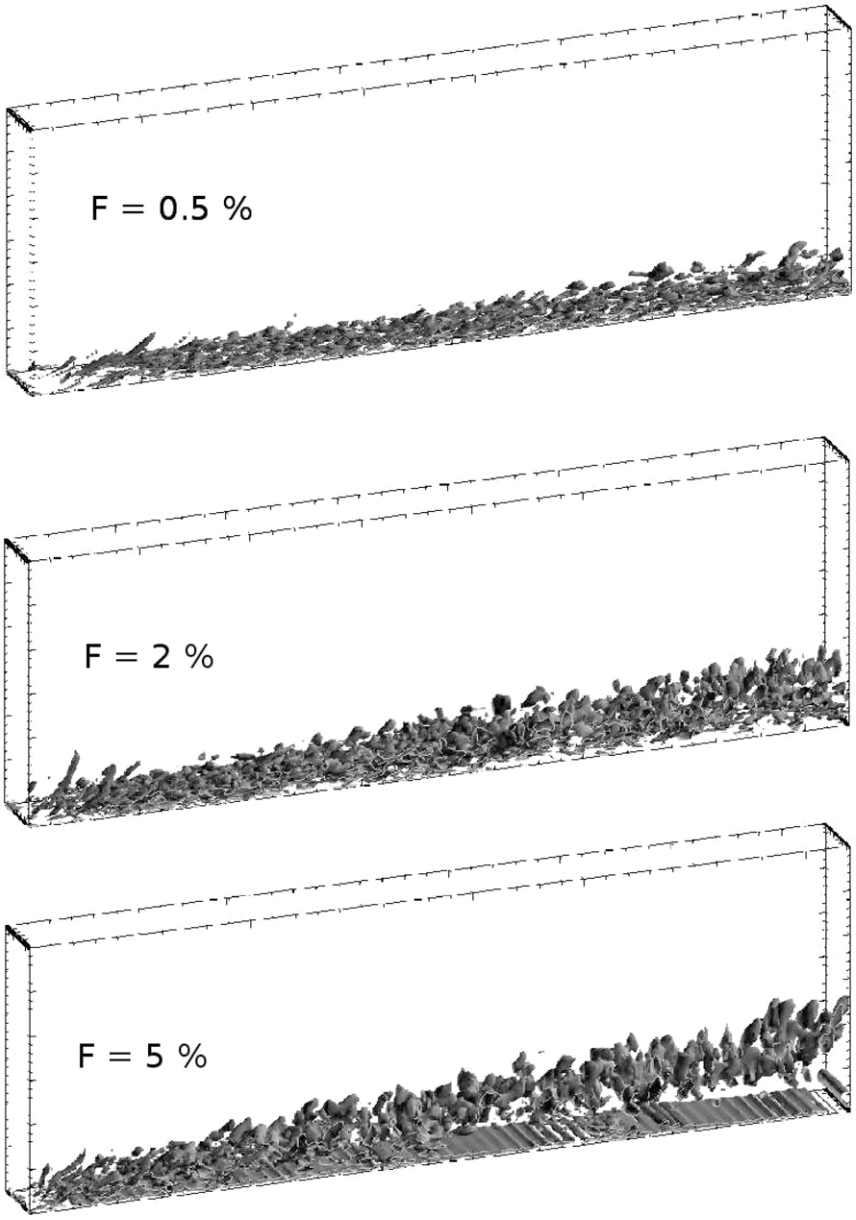

Fig. 7. Q criterion, threshold at 50,000 s^{-2}.

4.3. Simulations for F = 5%: blown off boundary layer

We carry out here a simulation for a higher blowing rate ($F = 5\%$). Previous work showed that at such a high blowing rate the boundary layer must be blown off (Bellettre et al., 2000). Indeed, the first simulations carried out at $F = 5\%$ showed this phenomenon. However, the initial domain appeared to be too small in that case since the boundary layer was "flattened" against the wall when compared to the experimental profiles. Consequently, the study of this blowing rate was made using a higher domain ($L_y = 0.24$ m instead of 0.12 m). The mesh was modified as well, in order to keep the same mesh resolution. The longitudinal velocity and temperature profiles obtained in that case are shown in Fig. 8.

We note a good agreement of the numerical and experimental data. The mean velocity profile is slightly over-estimated by the simulations. Nevertheless, the agreement is excellent knowing the difficulty to numerically reproduce the blow off. The fluctuation peaks are very well reproduced by our simulations, even better than with lower blowing rates. This is probably because the peaks are located farther away from the wall at $F = 5\%$ and thus are not affected by all the complex physical phenomena that take place for $y \leqslant 0.02$ m, especially the interaction of the main and injected flows. Indeed, the near-wall part of these rms profiles, before the peak, are not as close to the experimental data as the rest of the profiles. This leads us to the following conclusion already suggested by Na (2005). The similarity between the temperature and the velocity, which is implied by the use of a constant subgrid-scale Prandtl number, does not hold close to a wall submitted to blowing and a more sophisticated subgrid-scale model would probably give a better estimation of the near-wall fluctuations. In particular, a model based on a dynamic calculation of the thermal diffusivity might improve the accuracy of the rms profiles in the near-wall area.

We see on the mean profiles (Fig. 8a and c) that there is a change of concavity at $y \approx 0.02$ m. It shows that in the near-wall area the velocity and the temperature remain low. This behaviour is typical of the blow off of the boundary layer. Moreover, the blow

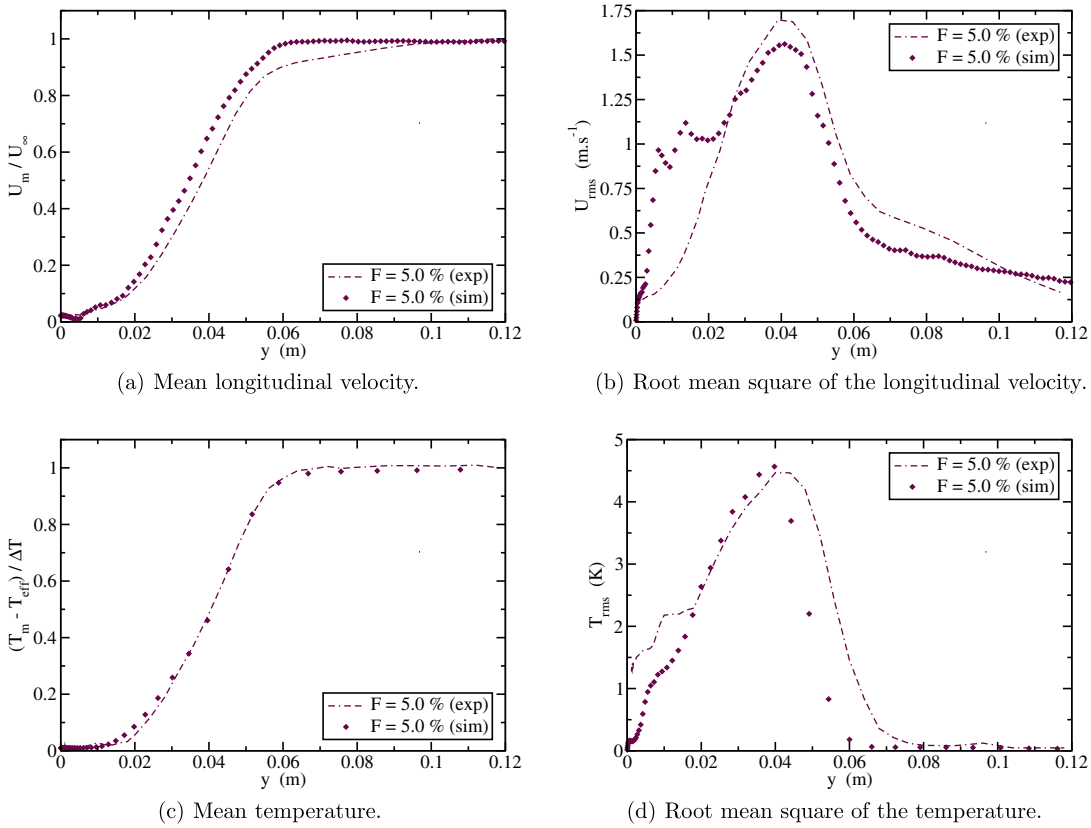

(a) Mean longitudinal velocity. (b) Root mean square of the longitudinal velocity.

(c) Mean temperature. (d) Root mean square of the temperature.

Fig. 8. Longitudinal velocity and temperature profiles ($F = 5\%$).

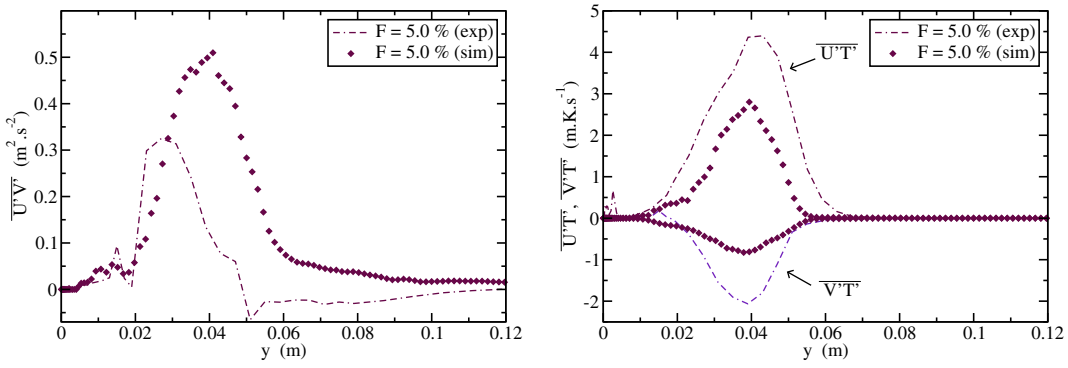

(a) Correlation $\overline{U'V'}$. (b) Correlations $\overline{U'T'}$ and $\overline{V'T'}$.

Fig. 9. Correlations profiles ($F = 5\%$).

off of the boundary layer for $F = 5\%$ is displayed by the Q criterion plot in Fig. 7, where we can see that the vortices of the boundary layer are separated from the wall. In this Figure, the rolls at the wall are a consequence of the "holes model" used to represent the porous plate. At such a high injection rate a swirl forms behind each transverse hole line. The fact that the peaks of the velocity and temperature fluctuations are farther away from the wall than with lower blowing rates is also a sign of the boundary layer blow off. The behaviour previously mentioned for the rms profiles is confirmed here: with this higher blowing rate the peaks are wider and their level is higher.

The velocity–velocity and velocity–temperature correlations are displayed in Fig. 9a and b. Discrepancies can be noticed between experimental and numerical curves even if simulations reproduce the curves shapes and peaks positions. The velocity–velocity correlation is positive. It was negative for lower blowing rates. The blow off of the boundary layer due to the strong injection induces a change in the near-wall turbulence: the velocity fluctuations dissipate momentum, while they produce momentum for lower blowing rates, illustrating the blow off physical phenomena.

5. Conclusion

We developed and tested a method based on parallel flows to simulate a developed thermal turbulent boundary layer. Tests in a turbulent plane channel showed that this inflow condition is very efficient. It produces appropriate profiles that are maintained downstream.

The Thermal Large Eddy Simulation was applied to the case of non-isothermal blowing through a porous plate. Comparisons of our numerical results with experimental data validate this turbulent inflow condition used in our simulations and showed that our mesh resolution is suitable. It was observed that blowing efficiently cools the wall, even at relatively low injection rates. The dynamic and thermal boundary layer thicknesses increase with the blowing rate and the fluctuations maxima increase and are shifted away from the plate. The boundary layer is blown off for $F = 5\%$. We had to use a higher domain at such a high blowing rate for this reason. This blow off was well reproduced by our simulations. The simulations also gave us access to new results like the transverse velocity fluctuations, the spatial evolution of the velocity and temperature and the Q criterion, which represents the turbulent structures of the flow.

References

Ackermann, C., Métais, O., 2001. A modified selective structure function subgrid-scale model. Journal of Turbulence 2 (11), 1–26.

Akselvoll, K., Moin, P., 1996. Large-eddy simulation of turbulent confined coannular jets. Journal of Fluid Mechanics 315, 387–411.

Bellettre, J., Bataille, F., Lallemand, A., 1999. A new approach for the study of turbulent boundary layers with blowing. International Journal of Heat and Mass Transfer 42 (15), 2905–2920.

Bellettre, J., Bataille, F., Rodet, J.-C., Lallemand, A., 2000. Thermal behaviour of porous plates subjected to air blowing. AIAA Journal of Thermophysics and Heat Transfer 14 (4), 523–532.

Brillant, G., Bataille, F., Ducros, F., 2004. Large-eddy simulation of a turbulent boundary layer with blowing. Theoretical and Computational Fluid Dynamics 17 (5–6), 433–443.

Brillant, G., Husson, S., Bataille, F., 2008. Experimental study of the blowing impact on a hot turbulent boundary layer. International Journal of Heat and Mass Transfer 51 (7–8), 1996–2005.

Chatelain, A., Ducros, F., Métais, O., 2004. LES of turbulent heat transfer: proper convection numerical schemes for temperature transport. International Journal for Numerical Methods in Fluids 44 (9), 1017–1044.

Dong, Y.-H., Lu, X.-Y., 2004. Large eddy simulation of a thermally stratified turbulent channel flow with temperature oscillation on the wall. International Journal of Heat and Mass Transfer 47, 2109–2122.

Dubief, Y., Delcayre, F., 2000. On coherent-vortex identification in turbulence. Journal of Turbulence 1, 1–21.

Ducros, F., Comte, P., Lesieur, M., 1996. Large-eddy simulation of transition to turbulence in a boundary layer developing spatially over a flat plane. Journal of Fluid Mechanics 236, 1–36.

Erlebacher, G., Hussaini, M.Y., Speziale, C.G., Zang, T.A., 1992. Toward the large-eddy simulation of compressible turbulent flows. Journal of Fluid Mechanics 238, 155–185.

Facchini, B., Ferrara, G., Innocenti, L., 2000. Blade cooling improvement for heavy duty gas turbine: the air coolant temperature reduction and the introduction of stream and mixed steam/air cooling. International Journal of Thermal Sciences 1, 74–84.

Germano, M., Piomelli, U., Moin, P., Cabot, W.H., 1991. A dynamic subgrid-scale eddy viscosity model. Physics of Fluids 3 (7), 1760–1765.

Jiménez, J., Moin, P., 1991. The minimal channel flow unit in near-wall turbulence. Journal of Fluid Mechanics 225, 213–240.

Kaltenbach, H.J., Fatica, M., Mittal, R., Lund, T.S., Moin, P., 1999. Study of the flow in a planar asymmetric diffuser using large-eddy simulation. Journal of Fluid Mechanics 390, 151–185.

Lee, S., Sanjiva, S.K., Moin, P., 1992. Simulation of spatially evolving turbulence and the applicability of Taylor's hypothesis in compressible flows. Physics of Fluids A 4 (7), 1521–1530.

Lee, J.S., Xu, W., Pletcher, H., 2004. Large eddy simulation of heated vertical annular pipe flow in fully developed turbulent mixed convection. International Journal of Heat and Mass Transfer 47, 437–446.

Le, H., Moin, P., Kim, J., 1997. Direct numerical simulation of turbulent flow over a backward-facing step. Journal of Fluid Mechanics 330, 349–374.

Lesieur, M., 1997. Tubulence in Fluids. Kluwer Academic Publisher.

Lund, T.S., Moin, P., 1996. Large-eddy simulation of a concave wall boundary layer. International Journal of Heat and Fluid Flow 17, 290–295.

Mathelin, L., Bataille, F., Lallemand, A., 2001a. Near wake of a circular cylinder submitted to blowing – I boundary layers evolution. International Journal of Heat and Mass Transfer 44, 3701–3708.

Mathelin, L., Bataille, F., Lallemand, A., 2001b. Near wake of a circular cylinder submitted to blowing – II impact on the dynamics. International Journal of Heat and Mass Transfer 44, 3701–3708.

Mellen, C.P., Frölich, J., Rodi, W., 2003. Lessons from lesfoil project on large-eddy simulation of flow around an airfoil. AIAA Journal 41 (4), 573–581.

Merkin, J.H., 1972. Free convection with blowing and suction. International Journal of Heat and Mass Transfer 15 (5), 989–999.

Merkin, J.H., 1975. The effects of blowing and suction on free convection boundary layers. International Journal of Heat and Mass Transfer 18 (2), 237–244.

Moin, P., 2002. Advances in large eddy simulation methodology for complex flows. International Journal of Heat and Fluid Flow 23, 710–720.

Moin, P., Kim, J., 1982. Numerical investigation of turbulent channel flow. Journal of Fluid Mechanics 118, 341–377.

Moin, P., Squires, K., Cabot, W., Lee, S., 1991. A dynamic subgrid-scale model for compressible turbulence and scalar transport. Physics of Fluids A 3, 2746–2757.

Montreuil, E., Sagaut, E., Labbé, O., 1999. Assessment of non-fickian subgrid-scale models for passive scalar in channel flow. In: Workshop on Direct and Large Eddy Simulation, Isaac Newton Institute for Mathematical Sciences.

Murata, A., Mochizuki, S., 2004a. Large eddy simulation of turbulent heat transfer in a rotating two-pass smooth square channel with sharp 180° turns. International Journal of Heat and Mass Transfer 47, 683–698.

Murata, A., Mochizuki, S., 2004b. Effect of rib orientation and channel rotation on turbulent heat transfer in a two-pass square channel with sharp 180° turns investigated by using large eddy simulation. International Journal of Heat and Mass Transfer 47, 2599–2618.

Na, Y., 2005. Direct numerical simulation of turbulent scalar field in a channel with wall injection. Numerical Heat Transfer Part A 47, 165–181.

Nicoud, F., Ducros, F., 1999. Subgrid-scale stress modelling based on the square of the velocity gradient tensor. Flow, Turbulence and Combustion 62, 183–200.

Peng, S.H., Davidson, L., 2002. On a subgrid-scale heat flux model for large-eddy simulation of turbulent thermal flow. International Journal of Heat and Mass Transfer 45, 1393–1405.

Piomelli, U., Balaras, E., 2002. Wall-layer models for large-eddy simulations. Annual Reviews of Fluids Mechanics 34, 349–374.

Rai, M.M., Moin, P., 1993. Direct numerical simulation of transition and turbulence in a spatially evolving boundary layer. Journal of Computational Physics 109, 169–192.

Rodi, W., 2006. DNS and LES of some engineering flows. Fluid dynamics research 38 (2–3), 145–173.

Sagaut, P., 2001. Large Eddy Simulation for Incompressible Flows: An Introduction. Springer-Verlag.

Sergent, A., Joubert, P., Le Quéré, P., 2003. Development of a local subgrid diffusivity model for large-eddy simulation of buoyancy-driven flows: application to a square differentially heated cavity. Numerical Heat Transfer Part A 44, 789–810.

Shima, N., 1993. Prediction of turbulent boundary layers with a second-moment closure: part I – effects of periodic pressure gradient, wall transpiration and free-stream turbulence. Journal of Fluid Engineering (ASME) 115 (1), 56–63.

Silva-Freire, A.P., Cruz, D.O.A., Pellegrini, C.C., 1995. Velocity and temperature distributions in compressible turbulent boundary layers with heat and mass transfer. International Journal of Heat and Mass Transfer 38 (13), 2507–2515.

Wang, W.P., Pletcher, R.H., 1996. On the large eddy simulation of a turbulent channel flow with significant heat transfer. Physics of Fluid 8 (12), 3354–3366.

Wu, X., Squires, K.D., Lund, T.S., 1995. Large-eddy simulation of a spatially developing boundary layer. In: ACM/IEEE Supercomputing Conference, San Diego, pp. 1–18.